Contrib Mineral Petrol (2011) 161:863–881
DOI 10.1007/s00410-010-0569-0

ORIGINAL PAPER

Enhancement of magma mixing efficiency by chaotic dynamics: an experimental study

Cristina P. De Campos · Diego Perugini · Werner Ertel-Ingrisch · Donald B. Dingwell · Giampiero Poli

Received: 15 March 2010 / Accepted: 4 August 2010 / Published online: 20 August 2010

Abstract Magma mixing is common in the Earth. Understanding the dynamics of the mixing process is necessary for dealing with the likely consequences of mixing events in the petrogenesis of igneous rocks and the physics of volcanic eruptive triggers. Here, a new apparatus has been developed in order to perform chaotic mixing experiments in systems of melts with high viscosity contrast. The apparatus consists of an outer and an inner cylinder, which can be independently rotated at finite strains to generate chaotic streamlines. The two cylinder axes are offset. Experiments have been performed for ca. 2 h, at 1,400°C under laminar fluid dynamic conditions ($Re \sim 10^{-7}$). Two end-member silicate melt compositions were synthesized: (1) a peralkaline haplogranite and (2) a haplobasalt. The viscosity ratio between these two melts was of the order of 10^3. Optical analysis of post-experimental samples reveals a complex pattern of mingled filaments forming a scale-invariant (i.e. fractal) distribution down to the μm-scale, as commonly observed in natural samples. This is due to the development in space and time of stretching and folding of the two melts. Chemical analysis shows strong non-linear correlations in inter-elemental plots. The original end-member compositions have nearly entirely disappeared from the filaments. The generation of thin layers of widely compositionally contrasting interfaces strongly enhances chemical diffusion producing a remarkable modulation of compositional fields over a short-length scale. Notably, diffusive fractionation generates highly heterogeneous pockets of melt, in which depletion or enrichment of chemical elements occur, depending on their potential to spread via chemical diffusion within the magma mixing system. Results presented in this work offer new insights into the complexity of processes expected to be operating during magma mixing and may have important petrological implications. In particular: (1) it is shown that, in contrast with current thinking, rheologically contrasting magmas can mix (i.e. with large proportions of felsic magmas and high viscosity ratios), thus extending significantly the spectrum of geological conditions under which magma mixing processes can occur efficiently; (2) the mixing process cannot be modeled using the classical linear two-end-member mixing model; and (3) the chemical compositions on short-length scales represent snapshots within the process of mixing and therefore may not reflect the final composition of the magmatic system. This study implies that microanalysis on short-length scales may provide misleading information on the parental composition of magmas.

Keywords Magma mixing · Chaotic dynamics · Experiments · Uphill diffusion · Geochemical variation

Communicated by T. L. Grove.

C. P. De Campos (✉) · W. Ertel-Ingrisch · D. B. Dingwell
Department of Earth and Environmental Sciences,
Ludwig Maximilians University, Theresienstrasse 41/III,
80333 Munich, Germany
e-mail: campos@min.uni-muenchen.de

D. Perugini · G. Poli
Department of Earth Sciences, University of Perugia,
Piazza Università, 06100 Perugia, Italy

Introduction

Magma mixing is a geological process of undoubted importance. Understanding its development, both in space and time, as well as inferring its end-products (i.e. mixed igneous rocks) is crucial for understanding such geological

processes on Earth, both near its surface and in its deeper interior. From a petrological point of view, studying the interaction between mafic and felsic magmas is often essential for deciphering the chemical composition of the primary melts. Constraints on crustal accretion processes greatly depend on recognition of the source regions for the magmas involved in the mixing processes (e.g. Wilson 1989; Bateman 1995; Christofides et al. 2007). From a volcanological point of view, the replenishment of a subvolcanic magma reservoir with less evolved magmas is considered to be one of the processes commonly triggering explosive eruptions (e.g. Sparks et al. 1977; Murphy et al. 1998; Leonard et al. 2002).

Since the first hypothesis for the origin of mixed igneous rocks (e.g. Bunsen 1851), ample evidence of magma mixing processes, in all tectonic environments, throughout geological times, has been recorded (e.g. Eichelberger 1978, 1980; Blundy and Sparks 1992; Wiebe 1994; De Campos et al. 2004a; Kratzmann et al. 2009). Field observations have been followed by geochemical, numerical, and low-temperature analogue models, using low-viscosity fluids (e.g. Fourcade and Allègre 1981; Huppert and Sparks 1984; Oldenburg et al. 1989; Snyder and Tait 1998; Jellinek et al. 1999; Bergantz 2000; Petrelli et al. 2006). These studies have provided an understanding of the basic dynamics associated with magma mixing and its potential in modulating geochemical variabilities in igneous systems. At this stage, the interplay between the turbulence of the system and the viscosity ratio between the mixing magmas has emerged as a decisive constraint for mixing efficiency (Jellinek et al. 1999). For the extreme case of rheological contrast involving a basaltic and granitic melt (a common occurrence in nature), such a constraint should drive mixing efficiency toward zero (Jellinek et al. 1999). As a consequence, petrologists generally assume that mingling, rather than chemical mixing, dominates the interaction between basaltic and granitic melts (e.g. Sparks and Marshall 1986; Bateman 1995).

To date, only a handful of experimental studies have focused on investigations with natural melts or magmas (e.g. Kouchi and Sunagawa 1984; Bindeman and Davis 1999; De Campos et al. 2004b, 2008) partly due to the high temperatures and high viscosities involved. Crucial in such experiments is the definition of mixing protocols, which should emulate real magma mixing scenarios under conditions of full experimental control of the flow field.

A conceptual framework for studying magma mixing, which is capable of addressing the complexity inherent to this highly non-linear process, is the investigation of mixing processes via chaos theory (e.g. Flinders and Clemens 1996; Bergantz 2000; Perugini et al. 2003, 2008; De Campos et al. 2010). These studies have revealed that the mixing of magmas can be elucidated by considering it as a chaotic process. Numerical models, based on chaos theory, can be used to quantify and reproduce features observed on natural outcrops (e.g. Perugini et al. 2003).

Here, we apply chaos theory to experimental magma mixing. We have performed the first controlled mixing experiment under chaotic dynamical conditions, using high-temperature melts with a high-viscosity contrast. For this purpose, a new experimental apparatus has been designed and constructed. Basalt- and granite-analog multicomponent silicate melts were mixed together, under controlled and reproducible chaotic conditions for approximately 2 h at 1,400°C.

After a brief introduction to the fundamental principles of chaotic mixing processes, we present our experimental apparatus, describe the performed experiment in detail, and discuss the results obtained in terms of mixing efficiency and potential petrological implications.

Mixing and chaos: basic principles

Below we introduce some basic principles of mixing and chaos which have influenced the development of our experimental apparatus.

Stretching and folding: the recipe for ‘mixing’ and ‘chaos’

The fundamental physical process producing mechanical mixing is the stretching and folding of two (or more) fluids in space. The stretching and folding process is also the basic dynamics leading to chaotic behavior. This in turn implies in the development of chaotic dynamics, which is therefore intrinsic to fluid mixing processes (e.g. Ottino 1989a; Aref and El Naschie 1995). For this reason, in the past few years there has been an increasing attention on the application of chaos theory to the study of fluid mixing (e.g. Ottino 1989a,b; Liu et al. 1994; Aref and El Naschie 1995). To visualize this process, Fig. 1 illustrates a fluid dynamic experiment, in which a black fluid is mixed with a white fluid. As the mixing time increases (from Fig. 1b to d), the original black square (Fig. 1a) is elongated and subsequently folded over upon itself, generating complex lamellar structures (or filaments; Fig. 1d). It is worth noting that such structures can range over many length scales producing scale-invariant ‘fractal’ patterns (e.g. Ottino et al. 1988; Ott and Antonsen 1989). This is a typical outcome, arising from the development, in space and time, of a chaotic process. The generation of filaments produced by mechanical stretching and folding of fluids, at several length scales (down to the micron-length scale), is a prerequisite for efficient mixing. This is because the contact area between fluids increases exponentially, resulting in

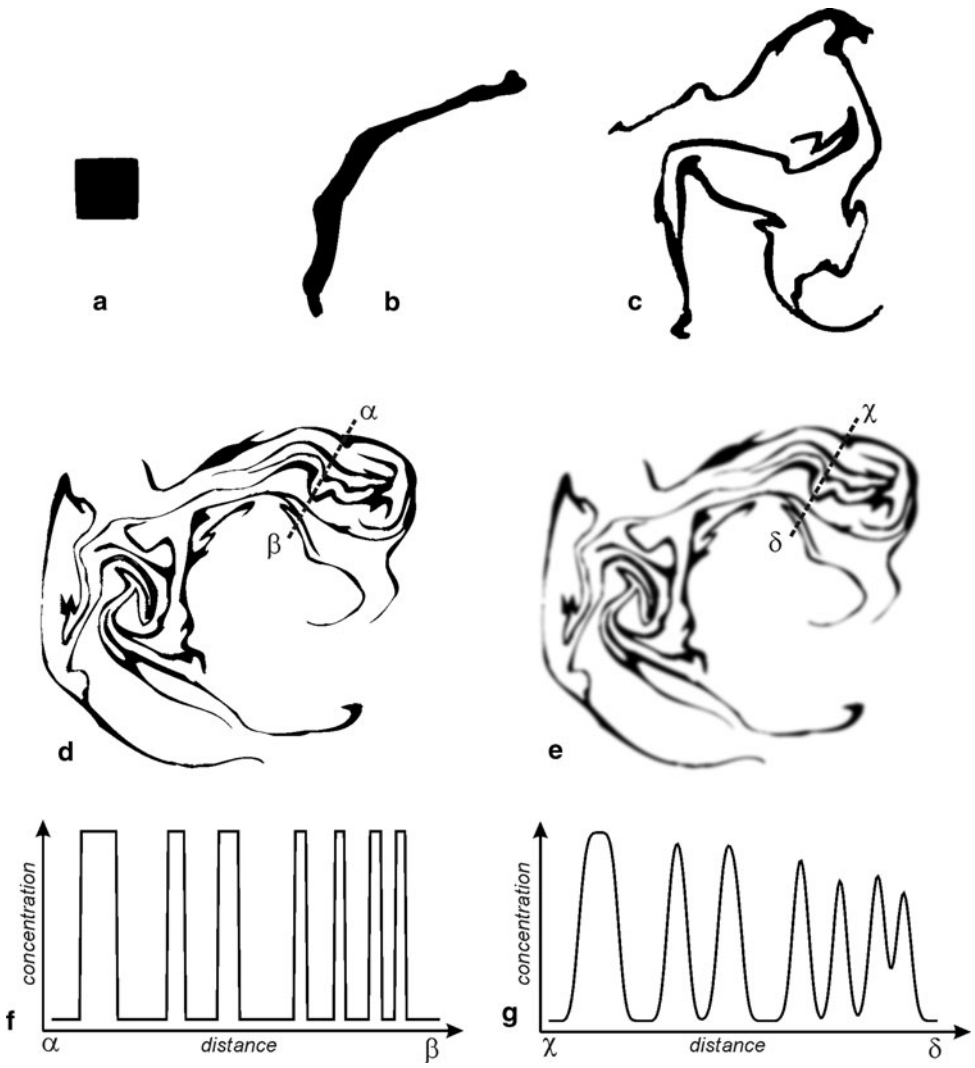

Fig. 1 **a–e** Stretching and folding dynamics acting on a *black colored square element* of contrasting fluids (from Welander 1955); the experiment was performed in a *rectangular* vessel of dimensions 50 × 30 × 30 cm filled with water to half the depth. On the water surface, a dark butanol film, corresponding to the *black square*, has been stirred by moving a square grid to produce the mixing pattern; **f**, **g** hypothetical compositional variation across the transects shown in **d** and **e** assuming the absence and presence of chemical diffusion, respectively

enhanced chemical exchanges through chemical diffusion processes (Fig. 1e, g).

Investigations into chaotic mixing of fluids

Much research has been carried out on chaotic mixing of fluids. A number of numerical models have been proposed, and many experiments have been carried out (e.g. Ottino 1989a; Liu et al. 1994; Aref and El Naschie 1995). In the numerical models, a class of dynamical systems, involving both advection (i.e. stretching and folding) and diffusion are typically employed (e.g. Ottino 1989b; Liu et al. 1994; Aref and El Naschie 1995). The use of these systems has helped to unravel the basic processes associated with this complex phenomenon and, in many cases, has provided the basis for setting up experimental protocols for the study of mixing processes using real fluids.

Several experiments have been developed to study chaotic mixing processes. These include the Taylor-Couette system (e.g. Akonur and Lueptow 2002), the cavity flow apparatus (e.g. Liu et al. 1994), and the journal bearing system (JBS; e.g. Swanson and Ottino 1990). The latter has received particular attention, as it enables the study of fluid mixing under careful control of the structure of flow fields via defined mixing protocols (e.g. Swanson and Ottino 1990; Galaktionov et al. 2002). We have therefore chosen the JBS to perform experimental mixing between silicate melts. It is perhaps worthwhile to describe the method here in some detail. Its basic geometry is shown in Fig. 2a. It consists of an outer cylinder, filled with the fluids of interest, and an inner cylinder, which is located off center. The geometry of the system is determined by two parameters: (a) the ratio of the radii of the two cylinders, $r = R_{in}/R_{out} = 1/3$, and (b) the eccentricity ratio to the outer cylinder $\varepsilon = \delta/R_{out} = 0.3$, where δ is the distance between the centers of the inner and outer cylinders (R_{in} and R_{out}). Rotating the cylinders in opposite directions triggers the mixing process; this dynamic protocol generates chaotic dynamics, since both

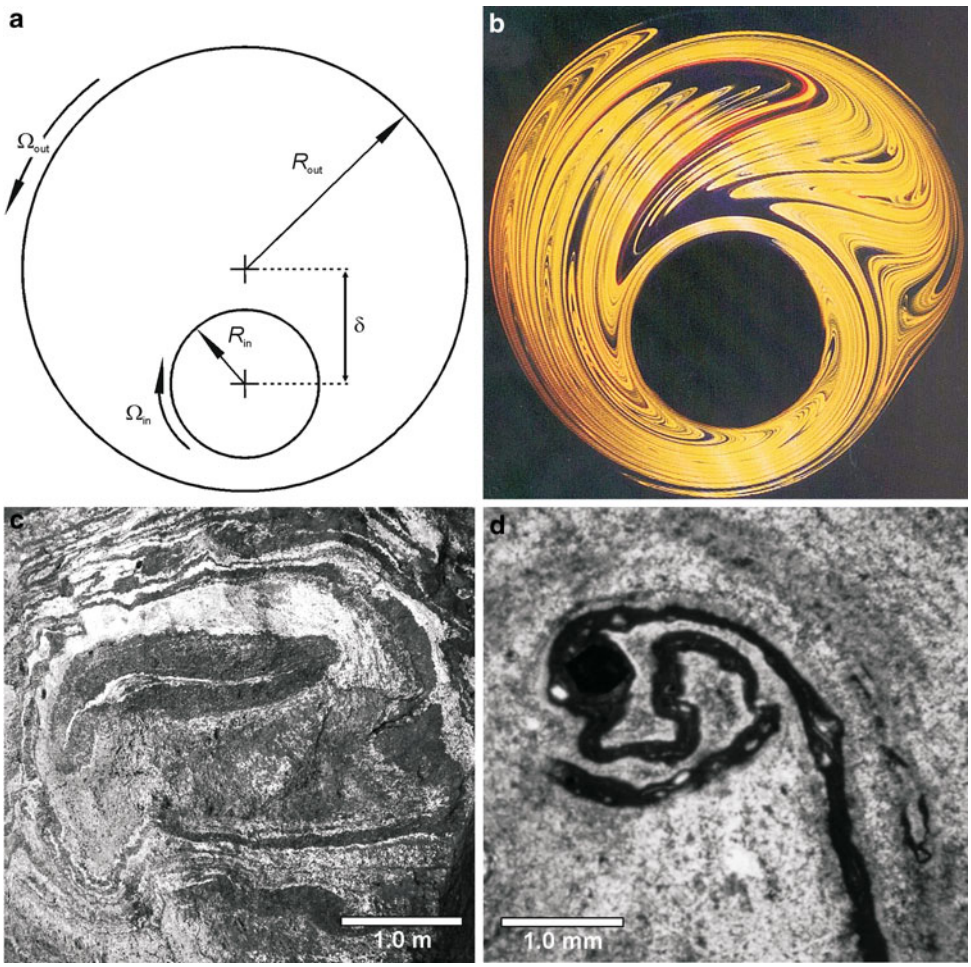

Fig. 2 **a** The Journal Bearing System geometry (JBS; e.g. Swanson and Ottino 1990); Ω_{in} and Ω_{out} are angular velocities of inner and outer cylinder, respectively; **b** Typical outcome of a mixing pattern, produced by the JBS (after Ottino et al. 1988) consisting of alternate rotations of both the outer and inner cylinder by an angular displacement of 270° for a duration of ten periods; host fluid is glycerin and the mixing pattern is due to stretching and folding processes of a fluorescent dye; **c**, **d** display of magma mixing structures from the Lesvos lava flow (Greece), at different length scales, where chaotic dynamics has been previously inferred (e.g. Perugini et al. 2003)

streamlines and velocity are time dependent (e.g. Swanson and Ottino 1990; Galaktionov et al. 2002). Typical experiments have been performed, at room temperature, by filling the outer cylinder with glycerin and introducing a fluorescent tracer to follow the induced flow fields. Note that viscosity ratio between fluids in this kind of experiment typically attains values of the order of 1.0 (i.e. the fluids have almost the same viscosity). Figure 2b displays a typical outcome from a JBS experiment (Ottino 1989b), in which, after a few rotations of the cylinders, a complex pattern of intimately mingled filaments emerges, due to the combined action of stretching and folding dynamics. The ability of the JBS to produce such an efficient mixing pattern, by fully controlling the mixing kinematics, makes it well suited for the experimental investigation into magma mixing processes.

Mixing of magmas

The study of several natural examples bearing evidence of magma interaction phenomena have repeatedly led to the inference that the magma mixing process can be defined as a chaotic process (e.g. Flinders and Clemens 1996; De Rosa et al. 2002; Poli and Perugini 2002; Perugini et al. 2003, 2006). From a kinematic point of view, the mixing of magmas is governed by the same stretching and folding processes which are responsible for (a) the development of chaotic dynamics in fluid mixing systems (Fig. 2c) and (b) the production of scale invariant (fractal) patterns, down to the micron-length scale (Fig. 2d), as expected for a chaotic process. The fact that magma mixing is a chaotic process means that its investigation can be reduced to the study of stretching and folding of those melts involved in the mixing process and, subsequently, to the onset of chemical diffusion. To date this approach has been undertaken mostly using simple numerical models, which have taken into consideration both advection (stretching and folding) and diffusion. This has enabled the investigation of the interplay between flow fields and the modulation of geochemical composition in the mixing system (e.g. Perugini et al. 2003, 2006). Despite the simplicity of such numerical methods, they are capable of generating structures and compositional patterns that mimic those observed in natural rocks. This observation confirms that a system

consisting of advection and diffusion contains much that is necessary for replicating the magma mixing process. Thus, irrespective of the specific processes responsible for advection (e.g. convection, flow in conduits, etc.), chaotic mixing of magmas is a very powerful conceptual tool for addressing the complexity of this petrogenetic process.

Guided by this conceptual model, we have developed the first experimental apparatus to reproduce experimentally chaotic mixing processes using high temperature silicate melts with strongly contrasting viscosities (i.e. similar to natural magmas). The experimental system contains all essential ingredients and fundamental building blocks to replicate the magma mixing process, including the production of stretching and folding processes between melts, the generation of scale-invariant (i.e. fractal) patterns and the onset of chemical diffusion processes. These properties make this new experimental system an important step toward an improved link between experiments and nature relative to previous experimental studies.

Experimental setup

The experimental apparatus

The apparatus used in this work is designed to accomplish two key objectives. First, to enable independent rotations of the inner and outer cylinder, at variable speeds, directions and stirring protocols, as in a typical JBS system and second, to place the apparatus in the hot spot region of a well-calibrated high-temperature oven, working at temperatures up to 1,700°C. In order to prevent secondary advection processes, associated with thermal convection, which could hinder the study of flow fields generated during mixing, the thermal gradient in the hot spot region did not vary by more than 0.5°C, at 1,400°C and $P = 1.0$ atm (i.e. the experimental conditions).

The experimental apparatus is technically based on the mechanically assisted equilibration technique (MAE) (Dingwell et al. 1994), initially used in geochemical solubility experiments and derived from concentric cylinder viscometry experiments (Dingwell and Virgo 1987, 1988). Earlier workers (e.g. Roeder 1974) used this method to homogenize experimental melts by mixing with a spindle rotated by an external motor at the top of the device (Fig. 3a). In this work, the MAE symmetry has been developed further to conform to the requirements of the JBS apparatus. Adding a driving mechanism at the bottom of the MAE device enables independent rotation of the outer cylinder (Fig. 3b–d). In addition, the driving mechanism of the spindle (i.e. the inner cylinder) at the top of the MAE device is positioned off-center to satisfy the JBS geometry ($r = 1/3$ and $\varepsilon = 0.3$). A 3D-sketch model and a

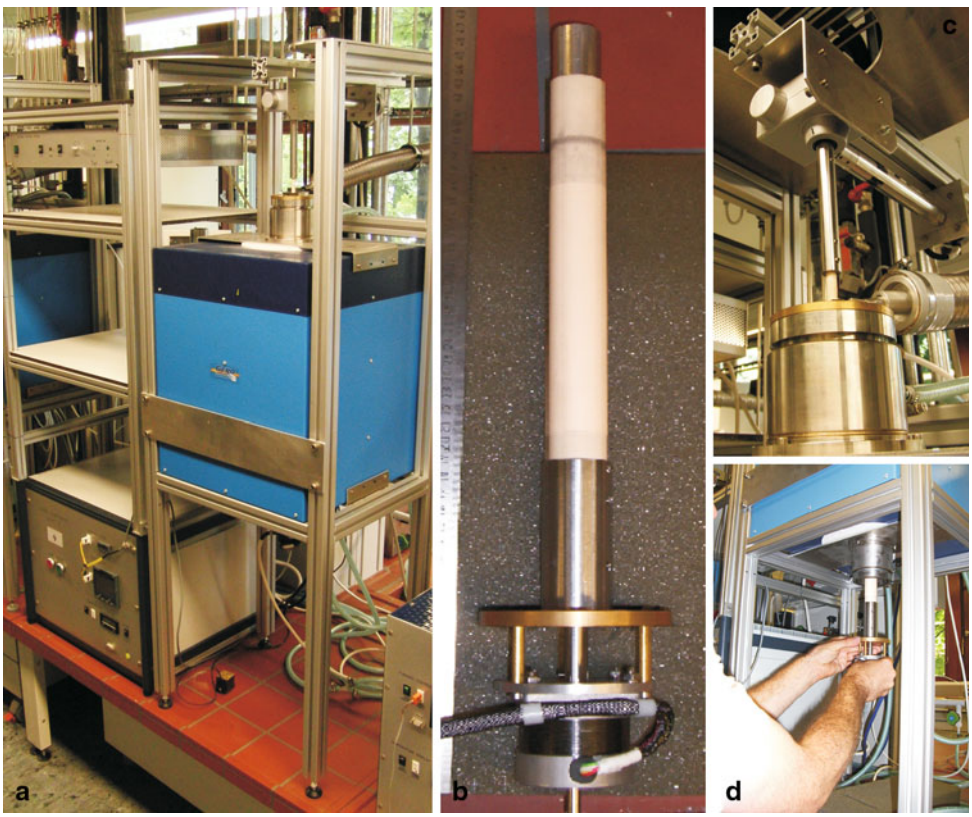

Fig. 3 The experimental apparatus: **a** oven overview; **b** lower motor with the Al_2O_3-rod and Pt_{80}-Rh_{20} connection to the outer cylinder (on the *top*); **c** upper motor with connection to the inner cylinder; **d** lower part of the insertion of the outer cylinder in the oven

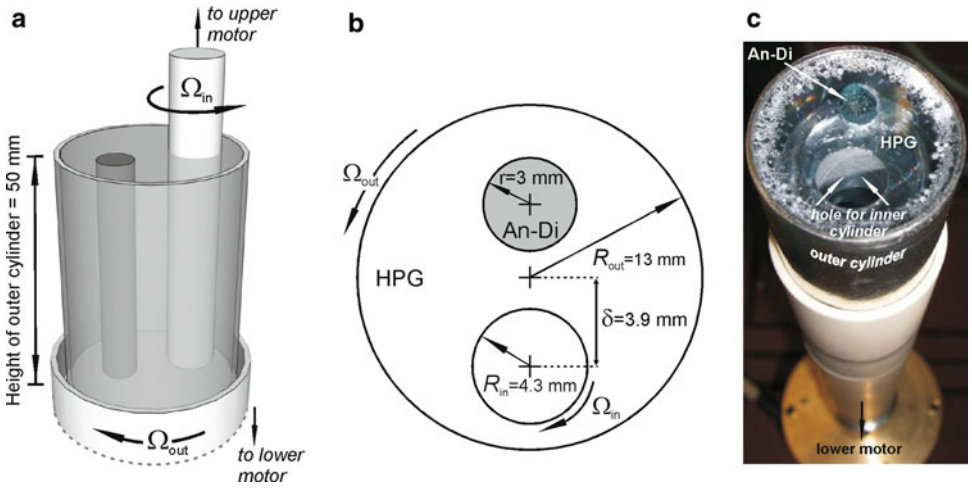

Fig. 4 **a**, **b** Schematic 3D-model and JBS cross section, used to perform experimental chaotic mixing of magmas; Ω_{in} and Ω_{out} are the angular velocities of inner and outer cylinder, respectively; **c** top view of the outer cylinder filled with the NK-HPG8 glass showing the location of the inner cylinder hole and An-Di glass; looking downwards, both the Al_2O_3-rod (*white color*) and lower motor can be seen

schematic cross section of the JBS used in this work are shown in Fig. 4a, b, respectively.

The motors for both (inner and outer) cylinder movements are controlled by a central mixing system, which enables independent control of rotation direction, rotation speed, and number of rotations. Prior to the start of an experiment, a mixing protocol is programmed. Protocol initiation starts the experiment (here at a constant temperature of 1,400°C).

Sample preparation and end-member compositions

The starting end-member materials consist of: (1) a peralkaline haplogranite melt (HPG8N5K5, hereafter NK-HPG8; Dingwell et al. 1998), and (2) a haplobasaltic melt composition corresponding to the 1-atm eutectic composition of the Anorthite-Diopside (An-Di) binary system. These two compositions are intended to act as analogs for the mixing of granitic and basaltic magmas in nature. Calculated viscosity values for the starting materials (after Giordano et al. 2008) at 1,400°C) are: NK-HPG8 ≈ 1,550 Pa s and An-Di ≈ 1.4 Pa s, resulting in a viscosity ratio of approximately 1.1×10^3, i.e. over three orders of magnitude higher than typical low-temperature JBS experiments (e.g. Swanson and Ottino 1990). NK-HPG8 and An-Di calculated densities (after Lange and Carmichael 1987) at 1,400°C are 2.26 and 2.52 g/cm^3, respectively. Mass fractions of the felsic and mafic melts for the experiment presented in this work are 94.5 and 5.5%, respectively.

For the preparation of the starting materials, oxides (for Si and Al) and carbonates (for K, Na, Ca and Mg) were used. Compositions of end-member glasses analyzed by electron microprobe (see "Geochemical variations in the mixing system" for analytical conditions) are given in Table 1.

Our experiment started with two homogeneous contrasting multi-component silicate melts. With time, the initial elemental concentrations in the end-members should drift toward the hybrid of this system. The estimation of the hybrid composition can be obtained by the classical two end-member mixing equation (e.g. Langmuir et al. 1978):

$$C_H^i = C_A^i x + C_B^i (1 - x) \quad (1)$$

where C_H^i, C_A^i and C_B^i are the concentrations of a given chemical element (i) in the hybrid, NK-HPG8 and An-Di, respectively, and x is the mass fraction of NK-HPG8 in the mixture. The concentration of the potential hybrid composition for each chemical element has been calculated by considering the end-member compositions reported in Table 1 and the original mass fractions of the two melts (i.e. 94.5% of NK-HPG8 and 5.5% of An-Di). These concentrations are a useful reference point in the discussion of the relative mobility of the different chemical elements during the mixing process.

Table 1 Composition (in weight%) of starting materials analyzed by electron microprobe (see "Geochemical variations in the mixing system" for details on analytical conditions) and calculated theoretical hybrid composition

Sample	SiO_2	Al_2O_3	MgO	CaO	Na_2O	K_2O
NK-HPG8 (*felsic end-member*)	70.28 ± 0.48	11.88 ± 0.18	b.d.l.	b.d.l.	8.27 ± 0.40	9.52 ± 0.18
An-Di (*mafic end-member*)	48.29 ± 0.34	15.90 ± 0.18	11.54 ± 0.12	24.11 ± 0.25	b.d.l.	b.d.l.
Theoretical hybrid composition	69.07 ± 0.46	12.10 ± 0.18	0.63 ± 0.03	1.33 ± 0.04	7.82 ± 0.38	9.00 ± 0.17

For the calculation of the hybrid composition element concentrations below detection limit (b.d.l.) are assumed to be zero. The range of compositions due to analytical uncertainties is also reported for each element

The experiment

Prior to the mixing experiment, NK-HPG8 and An-Di starting mixtures were fused separately inside $Pt_{80}Rh_{20}$ crucibles with a radius of 13.0 mm inside a MoSi2-heated box furnace. The resultant melts were homogenized at 1,600°C in air in a concentric cylinder viscometer for 7 days for the NK-HPG8 and, a couple of hours for An-Di. Both crucibles were then removed from the furnace and allowed to cool to room temperature.

Two cylinders were drilled out from the NK-HPG8 starting glass to obtain the required geometric configuration for the experiment (Fig. 4): one cylinder (with a radius of 4.3 mm) was cored out at the position of the future spindle (i.e. inner cylinder); a second cylinder ($r = 3.0$ mm) was cored at the future initial position of the An-Di cylinder. Prior to the experiment, a 50-mm (±1 mm)-long cylinder, drilled from the An-Di glass, was inserted into the NK-HPG8 glass (Fig. 4c). The crucible was then transferred into a vertical muffle tube furnace. An Al_2O_3-pedestal, which was connected to the motor below outside the furnace tube (Fig. 3), was used to position the crucible in the center of the hot spot region of the 1-atm gas-mixing furnace. The spindle (inner cylinder) was made of an alumina (AL23) rod and was sheathed at the lower end by a tight-fitting Pt foil. It was inserted into the hole inside the NK-HPG8 glass, which had already been transferred into the furnace. This inner cylinder was then connected to the motor above and outside the oven (Fig. 3c) and was located off-center, precisely at the required position of the JBS.

The furnace was heated up to run temperature (1,400°C) and held over approximately 45 min to allow NK-HPG8 and An-Di glasses to thermally relax. Then the experiment was initiated by turning on the experimental mixing protocol. The computer-controlled mixing protocol consisted of a combination of separated alternating rotations of the outer and inner cylinders in the following sequence: (1) two complete rotations of the outer cylinder in 36 min; (2) six complete rotations of the inner cylinder in 18 min; (3) two complete rotations of the outer cylinder in 36 min; (4) six complete rotations of the inner cylinder in 18 min. This combination of rotations ensures that chaotic streamlines develop, throughout the entire experimental system, leading to an efficient mixing without the formation of regular regions (Muzzio et al. 1992). The Reynolds number was calculated using:

$$Re = \rho VL/\mu \quad (2)$$

where V is characteristic velocity, $V = |V_{in}| - |V_{out}|$, with $V_{in} = \Omega_{in}R_{in}$ and $V_{out} = \Omega_{out}R_{out}$; L is a characteristic length $L = R_{out} - R_{in}$; ρ and μ are the density and viscosity and Ω_{in} and Ω_{out} are the angular velocities of inner and outer cylinder, respectively.

During the experiment, Reynolds number was of the order of 10^{-7} corresponding to laminar fluid-dynamic conditions, as required by the JBS system (e.g. Ottino 1989b). After the complete mixing protocol was finished, the experiment was terminated by switching off the power supply of the furnace, allowing the melt to cool to room temperature at an initial quench rate of ca. 80°C/min.

The crucible with the experimental charge was recovered from the gas mixing furnace by disconnecting the motor from the inner cylinder and extracting the outer cylinder from the bottom of the oven with the spindle (inner cylinder) still inside the sample. At room temperature, the alumina spindle could easily be removed from the Pt sheath with the latter remaining inside the outer cylinder within the experimental charge. The entire sample (including the Pt sheath) was recovered by coring out a cylinder with a radius of 11.0 mm from the crucible (outer cylinder). This core was then sectioned perpendicular to its long axis into 10 slices (Fig. 5a) for further analyses.

Results

Optical analyses

Figure 5b, c displays two representative sections (CD-25 and CD-26) collected by high-resolution transmitted light optical scanning of samples. CD-25 (thickness ca. 4 mm) is a section 20 mm above the lower end of the glass cylinder and CD-26 (thickness ca. 5.0 mm) is positioned 5.0 mm higher than the previous one (Fig. 5a).

Optical inspection of the sections confirms a crystal-free state. Several structural features present in the samples are worth discussing before moving to the illustration of mixing patterns. The first one is the occurrence of a thick and dark strip surrounding part of the inner cylinder (indicated by a white arrow in Fig. 5b, c). This is a glass fracture formed during quenching and removal of the sample from the crucible. Since pictures have been obtained by scanning thick samples, light diffracted along this fracture produces a dark appearing shadow. Furthermore, both samples display the occurence of bubbles. These bubbles constitute ca. 2% of the total sample volume and occur for two reasons: (1) due to the air trapped in the powdered samples during glass preparation (most of the bubbles have been drained from the melts during melt homogenization but some still remained in the final glass); (2) they formed during the melting step before the beginning of the experiment because of a thin film of air trapped between the NK-HPG8 glass and the inner cylinder and the An-Di glass. This is clearly indicated by the fact that many of them are concentrated around the inner cylinder (Fig. 5b, c). This occurrence is unavoidable due to the fact

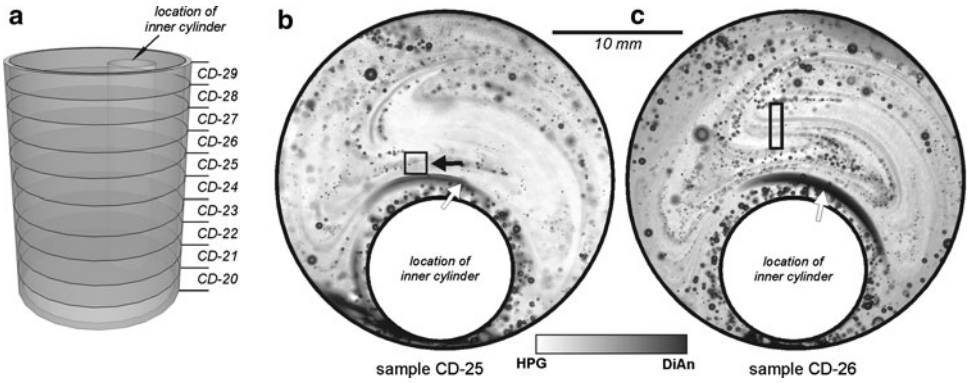

Fig. 5 **a** Schematic 3D-model of the experimental sample after quenching, showing the approximate location of sections extracted for further analyses; **b**, **c** transmitted light images of two representative sections. The *dark colored spots* of variable size in the two samples are vesicles. The *white arrow* in **b** and **c** indicates a dark strip corresponding to a fracture in the experimental sample (see text for details). The *black rectangular region* in **c** indicates the location of the compositional transect reported in Fig. 7. The *black square* in **b** is the approximate location of the chemical map presented in Fig. 11. This is highlighted by a *black arrow*

that the NK-HPG8 glass needs to be drilled for hosting the inner cylinder and An-Di glass (Fig. 4c).

The presence of bubbles in the experimental system may raise an additional question whether upward bubbles migration may perturb the flow field generated by cylinder rotation. To test this possibility, we calculated the distance travelled by bubbles during the time-scale of the experiment (i.e. 108 min). In particular, bubble ascent velocity has been calculated using the Stokes law (e.g. Lautze and Houghton 2007):

$$v_{\mathrm{b}} = \frac{2}{9}(\rho_{\mathrm{m}} - \rho_{\mathrm{b}})gR^2\left(\frac{1}{\eta_{\mathrm{m}}}\right) \tag{3}$$

where v_{b} is the bubble ascent velocity, g is the acceleration due to gravity, R is the bubble radius; ρ_b is the density of the bubble (~ 0), ρ_{m} is the melt density and η_{m} is the bulk magma viscosity. For these latter two parameters, we consider the values of the NK-HPG8 melt (i.e. $\rho_{\mathrm{b}} = 2.26$ g/cm^3 and $\eta_{\mathrm{m}} = 1{,}550$ Pa s) as it constitutes ca. 95% of the sample. We also consider a bubble diameter of 0.15 mm, i.e. the average diameter of bubbles occurring in the sample. Results indicate that for the time-scale of the experiment, an average bubble would rise ca. 100 μm in the melt column. Taking into account the filaments length produced by cylinder rotation (of the order of several decimeters), the effect of potential bubble induced mingling can be considered very minimal. This is further supported by the observation that bubbles are passively transported by flow fields as evidenced by the fact that they are aligned along streamlines (Fig. 5b, c). These calculations and observations indicate that the impact of bubbles on the flow fields generated during this experiment can be considered negligible.

Focussing on the mixing patterns obtained in the experimental samples: they disclose a complex pattern of lamellar structures, distributed throughout the mixed system. The development of stretching and folding processes and, hence, the development of chaotic dynamics, induced by the eccentric cylindric geometry of the JBS, is evidenced by vortex-like structures, consisting of alternations of filaments from the two melts. Comparison between the patterns in Fig. 5c, d and those produced by mixing of low-viscosity fluids (Fig. 2b) clearly evidences a similarity of spatial distribution of structures indicating that our chaotic mixing experiment using high-viscosity melts under high temperatures reproduces the general character of low-temperature analog fluid experiments (i.e. the formation of a great number of filaments of melts/fluids). When Fig. 5b is compared to Fig. 5c, it seems that a greater amount of filaments is present in Fig. 5c. This effect is only apparent and is due to the lower thickness of Fig. 5b (4.0 mm) relative to Fig. 5c (5.0 mm) which produced a different response of the sample when crossed by the transmitted light used in the image acquisition. The symmetry of the experiment does not allow the production of different flow fields at different depths (Swanson and Ottino 1990), but, on the contrary, the flow field is maintained constant throughout the whole length of the cylinder, with the exception of the very bottom of the cylinder, a system portion lying far away from the analyzed section and that, therefore, does not influence results presented in this study.

Structural analysis

Given that filaments are the most evident structural feature arising from the mixing process, we performed their quantitative analysis. In particular, several authors indicated that the thickness of filaments generated during chaotic mixing processes (e.g. Allègre and Turcotte 1986; Toramaru et al. 2001) is expected to follow a fractal scale-invariant distribution of the form:

$$N_c = \delta^{-b} + c \quad (4)$$

where N_c is the number of filaments with a thickness greater than δ, b is the power-law exponent and c is a constant. Writing Eq. 4 in logarithmic form we obtain:

$$\log(N_c) = -b\log(\delta) + \log(c) \quad (5)$$

implying that, in order to obtain a scale-invariant distribution, the cumulative frequency distribution of widths (N_c) of filaments has to be linearly correlated with δ in a log–log plot, with b being the scaling exponent. The scale invariant property of the experimental sample has been investigated using the cumulative frequency distribution of widths the mafic melt (i.e. An–Di). Filament thickness has been measured by image analysis on a number of sample sections, and Fig. 6 displays obtained results. The graph shows that data points are aligned along a straight line, clearly indicating that the chaotic advection protocol, used in this work to promote mixing between the two melts, generated a scale-invariant (i.e. fractal) distribution of filaments. The scaling exponent $b = -0.91$ quantifies the extent of scale invariance in the studied system.

Geochemical variations in the mixing system

In order to document the compositional variability produced by the mixing process, a transect through filaments occurring in sample CD-26 (Figs. 5c, 7) has been investigated. In addition, elemental maps have been collected in sample CD-25 (Figs. 5b, 11) over an area of ca. 4.0 mm^2,

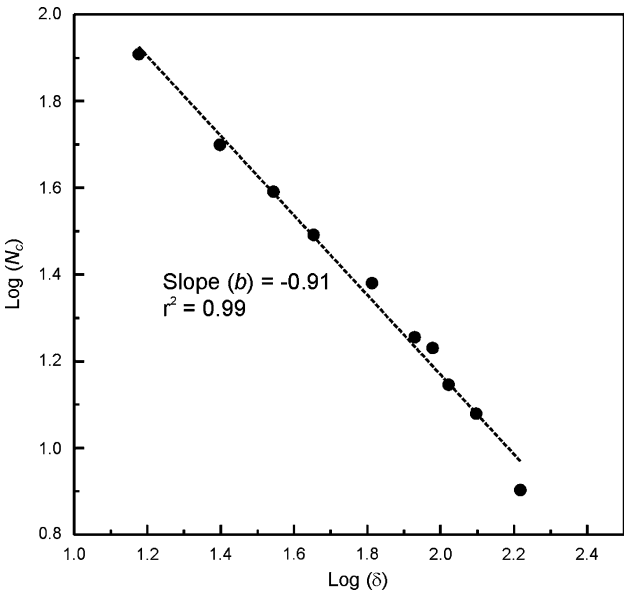

Fig. 6 Variation of the number of filaments (N_c) of the mafic melts with a thickness greater than δ as a function of δ showing the scale-invariant (i.e. fractal) nature of mixing structures produced by the present chaotic mixing experiment

in which a filament of An-Di was clearly visible. Chemical compositions were measured with a Cameca SX100 (Earth and Environment, LMU—Munich). The electron microprobe operating conditions were 15 kV acceleration voltage and 20 nA beam current. A defocused 10-μm beam was used for all elements in order to avoid alkali loss. Synthetic wollastonite (Ca, Si), periclase (Mg), corundum (Al), natural orthoclase (K), and albite (Na) were used as standards, and matrix correction was performed by PAP procedure (Pouchou and Pichoir 1984). Standard deviations were lower than 2.5% for all analyzed elements. Operating conditions for the collection of elemental maps were the same as above, using a dwell time of 0.4 s for all elements.

Figure 7 displays the variation of major element concentrations along the transect running across the filaments produced by the mixing process (i.e. across a diffusive boundary layer). A flat pattern corresponds to the abundances of elements in the felsic end-member. In contrast, in the central part compositional jumps can be observed. These are the resultant filaments originated from the combined action of (1) stretching and thinning of compositional interfaces, which are produced by the mechanical mixing and, (2) chemical diffusion. More detailed observations indicate that all analyzed elements share some common features, which are related to the occurrence of three main filaments, crossed by the transect (Fig. 7). The behavior of the different elements is, however, individual, with respect to modulation via this mixing pattern. Consider SiO_2 and Al_2O_3: since the An-Di end-member is richer in Al_2O_3 and poorer in SiO_2 relative to the NK-HPG8, one would expect that these oxides would display opposing fluxes. This is roughly the case along the profile with the exception of the region around 1.0 mm, where the first filament starts. Here, Al_2O_3 first decreases, defining an uphill diffusion trend (e.g. Watson and Jurewicz 1984) and then increases forming a first bell-shaped pattern reaching a maximum at ca. 13.0% followed by a second and narrower bell-shaped peak, with a maximum at ca. 14.5%. The SiO_2-variation pattern appears to be more coherent. All three peaks point toward lower values (i.e. toward the mafic end-member). However, in contrast to Al_2O_3, these peaks are not sharply separated. They coalesce instead and partially overlap. Na_2O mimics the Al_2O_3-pattern, to some extent. The major difference is a stronger uphill diffusion effect emerging at both ends of the segment considered. Shape and thickness of the second and third peaks for Na_2O are very similar to those displayed by Al_2O_3. The K_2O-compositional-pattern appears noisier with the presence of the three weak peaks pointing toward lower concentrations (i.e. toward the mafic end-member) and resembles the SiO_2-pattern. CaO and MgO show very similar behavior. However, CaO depicts a smoother pattern than MgO across

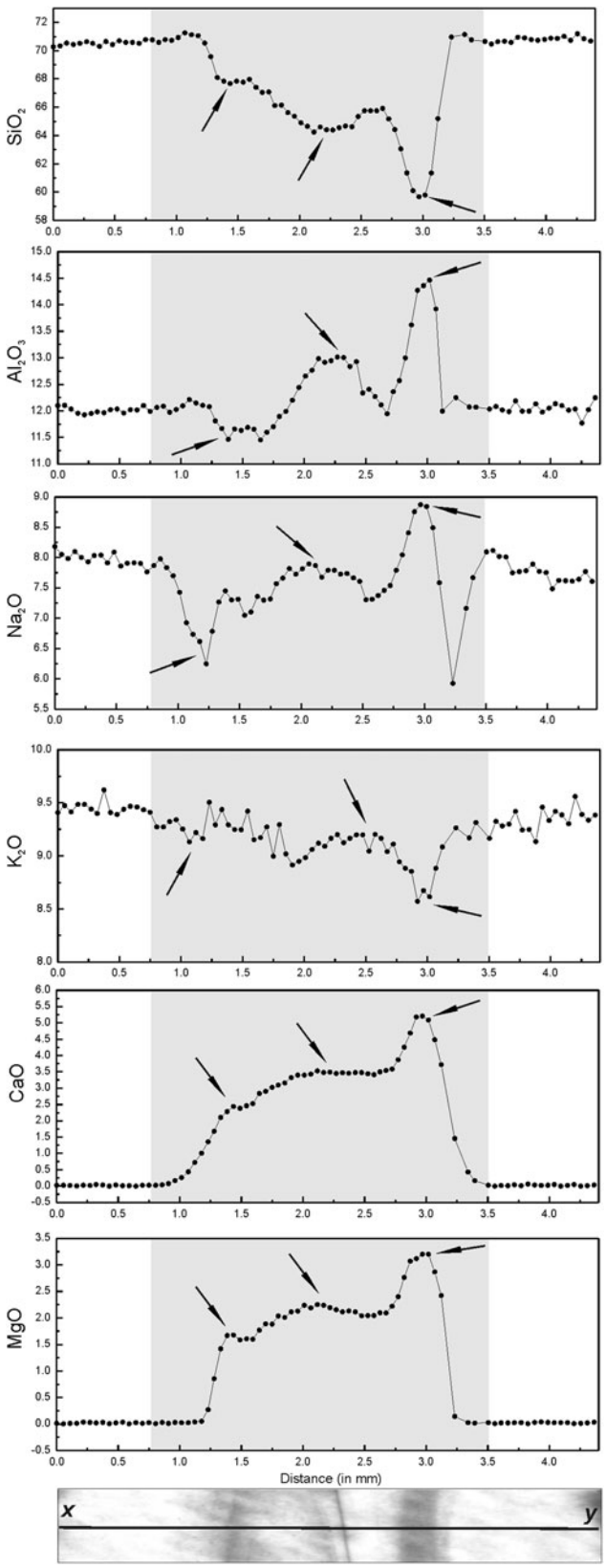

Fig. 7 Variation of analyzed elements along a transect crossing ▶ filaments in the experimental sample. The panel at the bottom of the figure reports a zoom in the region marked by the black rectangle in Fig. 5c and shows the exact location of the transect in the experimental sample

the first two filaments that almost totally coalesce and are not readily distinguishable. The third peak is evident for both elements.

An important observation emerging from the plots in Fig. 7 is that the original end-member compositions have nearly entirely disappeared from the filaments. To better appreciate this result, compositional histograms have been constructed (Fig. 8) using compositional data from the region where changes in composition were detected (i.e. between 0.8 and 3.5 mm in Fig. 7). For comparison, the original end-members, as well as the theoretical hybrid composition, are reported in the histograms (Fig. 8). As pointed out by Perugini et al. (2004), compositional histograms for a mixing system undergoing chaotic advection/diffusion processes should evolve from the original end-member compositions (i.e. the compositional histogram is constituted by two populations of concentrations, corresponding to the two initial end-members) to a bell-shape, whose maximum corresponds to the hybrid composition. If the mixing process is eventually completed (i.e. a homogeneous volume of melt with the hybrid composition is generated), the compositional spectrum collapses to a single population, whose concentration coincides with the hybrid composition. As can be seen in Fig. 8, there are no traces of the initial composition of the mafic end-member for any of the studied chemical elements. Also the composition of the felsic end-member is strongly shifted, with only a few samples falling in the field of its original composition. Most of the sample population exhibits intermediate values between the two end-members, with the different element distributions lying at different positions, relative to the theoretical hybrid. In particular, it can be said that the distributions of CaO and MgO are those lying farther away from the hybrid composition, followed by SiO_2 and Al_2O_3. Na_2O and K_2O, in contrast, display a larger number of data points falling in the range of values of the expected hybrid.

To better understand element variations in the studied mixing system, inter-elemental binary plots have been constructed with the same data set used in Fig. 8. They are shown in Fig. 9. In particular, the plots on the left-side display analyzed samples plus both end-members, whereas on the right side a zoom into the area covered by data points (gray area in the plots on the left side) is shown. A classical conceptual model invoked when dealing with magma mixing processes is that linear correlations must be observed in any inter-elemental binary diagram, irrespective of the chosen couple of elements. This idea comes from the application of Eq. 1, which predicts linear variations in inter-elemental plots. Observation of the plots in Fig. 9 indicates that this is not clearly the case: element

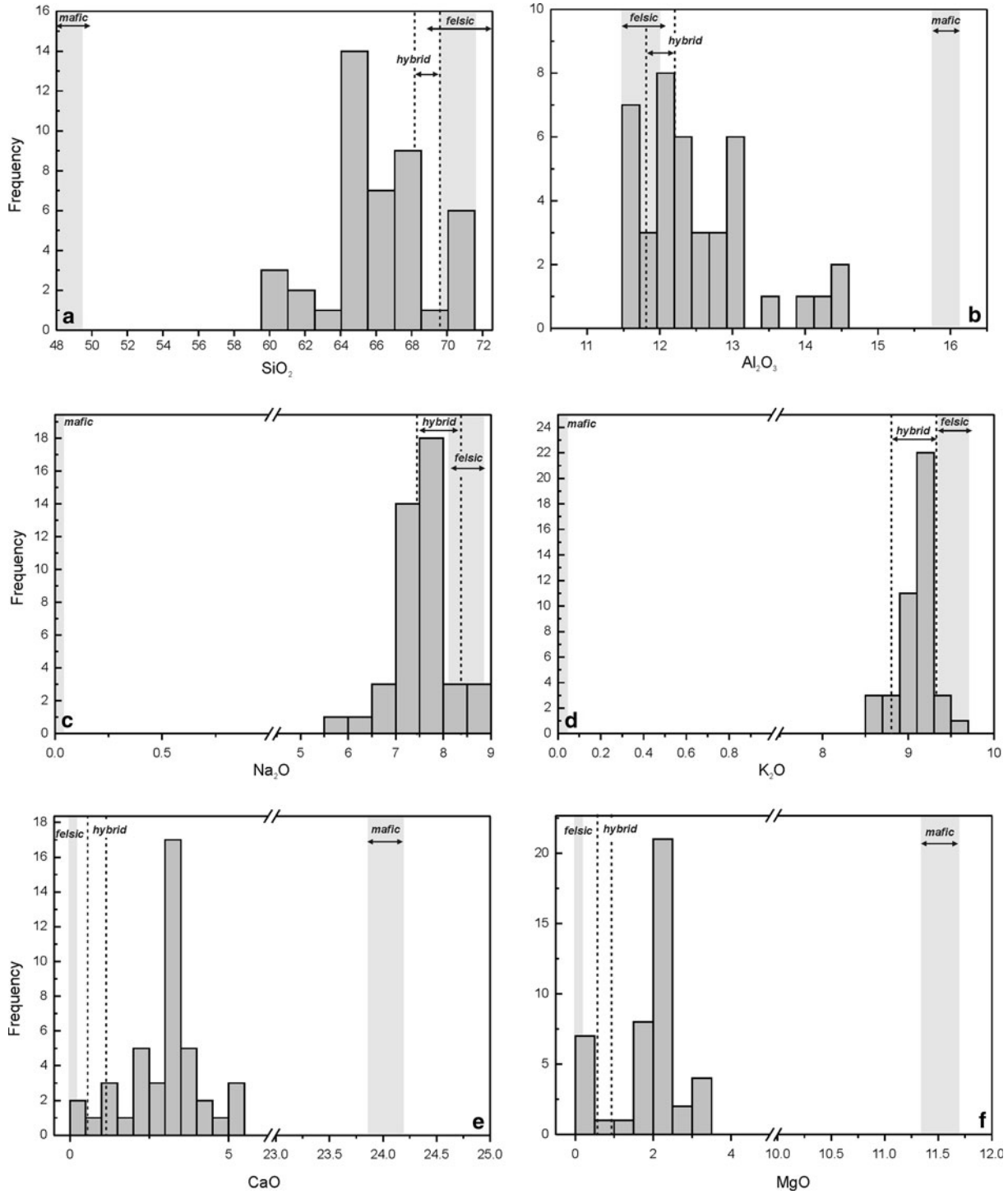

Fig. 8 Frequency histograms of compositional variability of analyzed chemical elements in the portion of the transect marked by a *shaded area*, in the CaO plot of Fig. 7. In the histograms, the original end-member as well as the theoretical hybrid composition is also reported, as shaded areas, considering the uncertainties of the microprobe analyses (Table 1). Element concentrations are given in weight%

variations occur as complex curvilinear patterns that strongly deviate from the mixing line connecting the end-members. Therefore, although the experiment has been performed by mixing two end-members, it did not generate the linear correlations that would be expected by the application of Eq. 1. On the contrary, inter-elemental correlations display a very large variability at the same time and in the same mixing system.

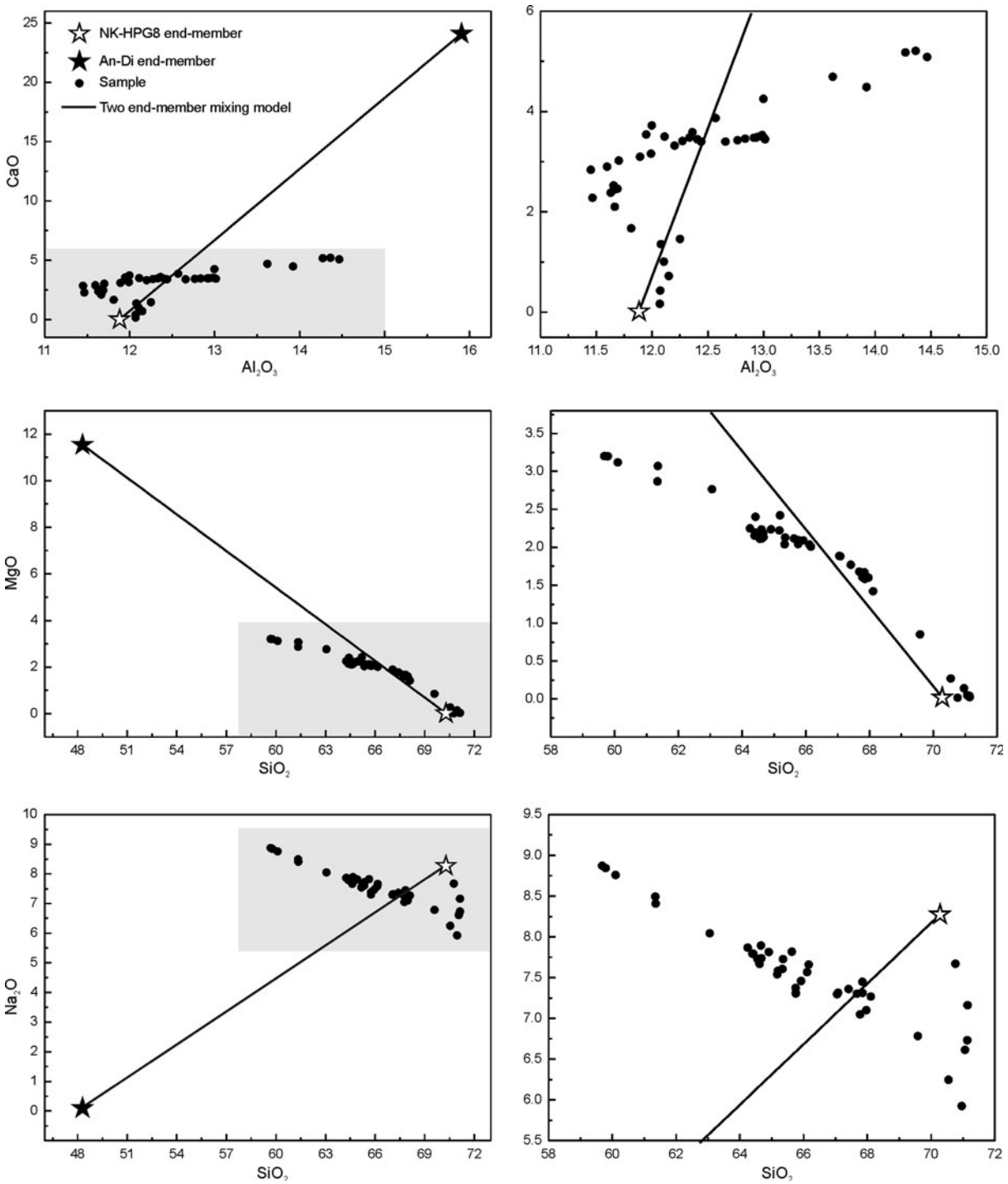

Fig. 9 Binary inter-elemental plots showing the geochemical variability in the experimental sample. Plots on the left side display analyzed samples plus both end-members, whereas the right side is a zooming into the area covered by data points (*gray area* in the plots on the left side)

A further feature, indicating deviation of our experimental system from the classical concept of two end-member mixing, is given by the application of the so-called "mixing test" proposed by Fourcade and Allègre (1981). Such a test is commonly used to assess the occurrence of magma mixing processes in petrology (e.g. Janoušek et al. 2000; Solgadi et al. 2007). The mixing test is performed by plotting the difference in all chemical elements between the most evolved (NK-HPG8) and least evolved (An-Di) end-member (i.e. $C_A - C_B$) vs. the difference in all chemical elements of a supposed hybrid composition and the least evolved (An-Di) end-member (i.e. $C_H - C_B$). Linear

interpolation of data points gives a twofold information: (1) the correlation coefficient (r^2), whose value indicates if the supposed hybrid sample can be regarded as the product of mixing—i.e. the larger the r^2 value, the stronger the evidence that the sample has a hybrid composition; (2) the slope of the linear fitting (x), which gives the proportion of the most evolved end-member in the mixture. The mixing test equation is derived from Eq. 1, by rearranging variables is such a way that:

$$C^i_H - C^i_B = x\left(C^i_A - C^i_B\right). \quad (6)$$

Plotting $C^i_A - C^i_B$ vs. $C^i_H - C^i_B$ (for simplification $C_A - C_B$ vs. $C_H - C_B$) and performing a linear interpolation of data gives the parameters of interest (i.e. r^2 and x). As reported above, application of this test requires the choice of a sample which is supposed to have attained the hybrid composition. The composition of the two original end-members and their relative mass proportions in the mixture are known and, therefore, the theoretical hybrid composition for each element can be calculated (Table 1). Then, from the available data set, samples displaying the hybrid composition for a given chemical element were selected. The choice of samples containing elements with the hybrid composition has been made considering the error associated with microprobe analysis, implying that an element is considered to have attained the hybrid composition if its concentration is in the range ±2.5% with respect to the measured concentration. Some representative plots resulting from the application of the mixing test considering as reference the hybrid concentrations of K_2O, Al_2O_3, and CaO are reported on left side of Fig. 10. Note that on $C_A - C_B$ vs. $C_H - C_B$ diagrams, only a portion of the plot can be populated by chemical elements for a two end-member mixing process; this portion, represented in the white color in Fig. 10, is bounded by the lines with slope $x = 1.0$ (i.e. the system is totally constituted by end-member 'A') and $x = 0.0$ (i.e. the system is totally constituted by end-member 'B'). These graphs indicate that all elements fall in the region associated with a two end-member mixing process and that the correlation coefficients are all very high. At first sight, this result may indicate that the selected samples have reached the hybrid compositions for all analyzed chemical elements. However, more detailed observations indicate that the estimated proportion of the least evolved end-member 'A' (i.e. the slope x of the linear interpolation) does not fit with the actual value (i.e. $x = 0.945$). In fact, it is clear that the claimed end-member 'A' proportion, considering as hybrid reference elements K_2O, Al_2O_3, and CaO, are $x = 0.854$, $x = 0.862$ and $x = 0.871$, respectively. These estimates are different from the true value (i.e. $x = 0.945$; dashed line in the plots) leading to errors in the proportion estimation of end-member 'A' of the order of 10%. Note that, although only some samples are displayed in Fig. 10, this is the case for all samples in which at least one element has reached the hybrid composition.

The right side of Fig. 10 reports the fraction of end-member 'A' claimed by each element. In other words, the calculated x-value for each element, from the left-side plots, is reported as a "spider diagram" on the right side. These plots show a striking x-value variability for different chemical elements. Values are shifted up to 20% with respect to the actual value (marked in the plots by the dashed line). This indicates that the sample suspected to be a hybrid for one element (e.g. K_2O, Al_2O_3 or CaO) does not have a hybrid composition for most of the other elements.

Figure 11a displays a false color image of a curved portion of another filament generated by stretching and folding dynamics in the studied mixing system. Chemical mapping has been performed on the an area of 2 mm vs 2 mm marked as a black quadrangle on sample CD-25 in Fig. 5b. Figure 11b, c, and d, reports the compositional variation in this portion of system for Mg, Ca and Na, respectively. Compositional variation for these three elements is reported as 3D-graphs, where the x and y coordinates represent the spatial dimensions of the mapped area and the z coordinate reports the concentration of the considered element. Regarding Mg, the compositional field describes a bell shape following the distribution of the filament in the mapped area, as expected from a typical diffusive process. Ca shows a slightly more complex pattern, with a sharper bell-shaped distribution and an additional compositional valley. Uphill diffusion follows the filament length along its middle path. The Na-pattern is roughly symmetrical relative to Ca, with a larger bell-shaped distribution at the center of the filament, which gradually evolves into two uphill diffusion valleys, at the external portions of the filament. Note that, also in the case of a single filament, the original composition of both end-members has been erased by chemical exchanges between the two melts in the vicinity of the filament.

From the above discussion, four main conclusions may be reached: (a) different chemical elements, although roughly following the structures from the mixing system (i.e. the filaments), define different compositional patterns; (b) the mixing process does not generate linear correlations as it should be expected from a typical two end-member mixing processes; (c) uphill diffusion in this system is experimentally confirmed during the mixing process and it strongly enhances the formation of heterogeneities in the system; (d) both original end-member compositions have almost vanished from the mixing system, where intimate mixing has occurred.

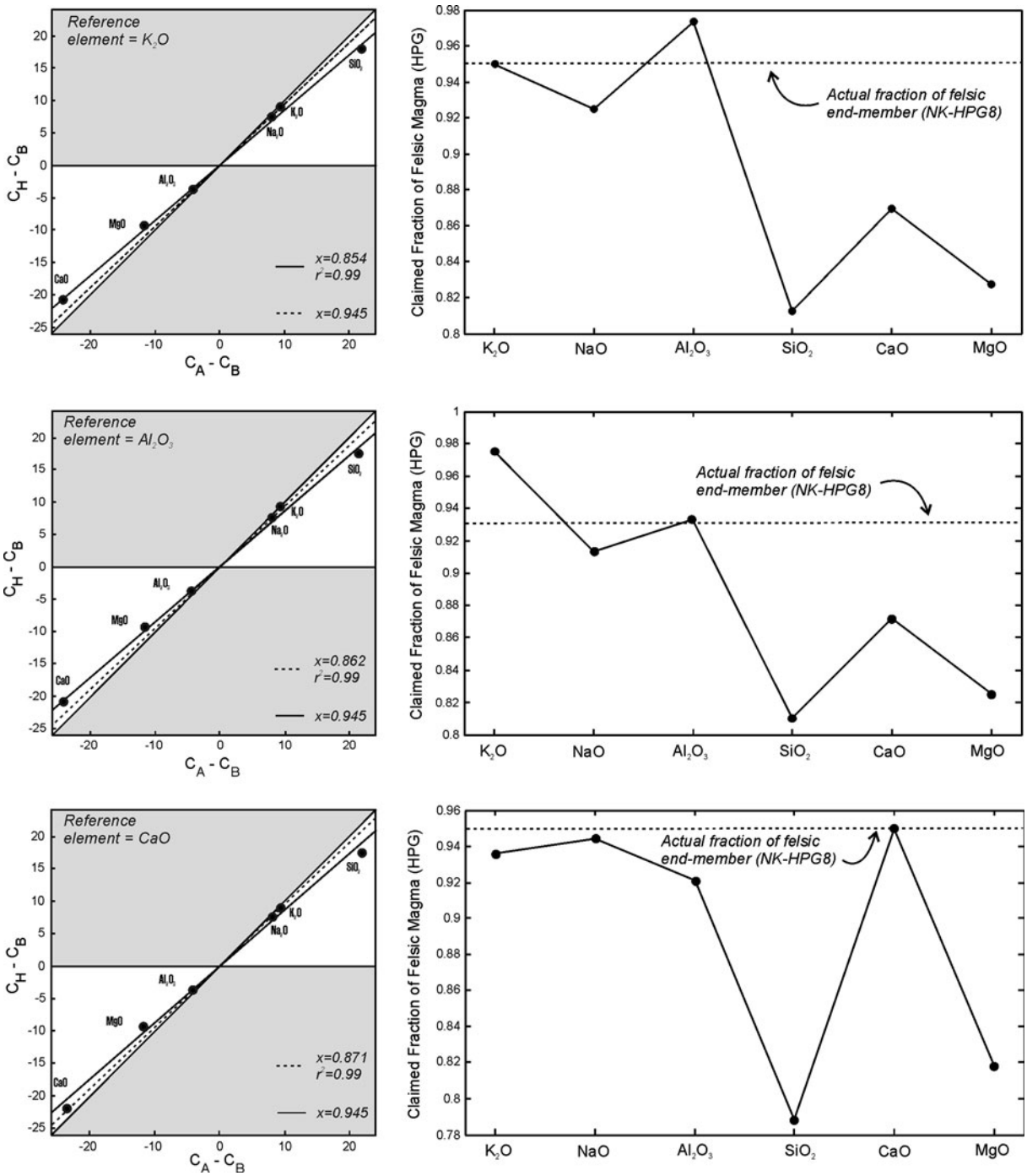

Fig. 10 *Left side* representative plots resulting from the application of the "mixing test" (Fourcade and Allègre 1981) considering as reference the hybrid concentrations of K_2O, Al_2O_3 and CaO; (*right side*) plots displaying the fraction of end-member 'A' (x) claimed by each element (see text for details)

Regarding the first three points, it must be kept in mind that different chemical elements may have different mobility in the same magmatic system (e.g. Hofmann 1980; Dingwell 1990; Baker 1990; Chakraborty 1995; Chakraborty et al. 1995; Mungall and Dingwell 1997); this effect can be amplified in multi-component systems, such as those used as end-members in the present work due to the nature of chemical diffusion. It is known for example that alkalis (Na and K) tend to have a higher mobility than other elements, because of their higher diffusivities (Hofmann 1980; Dingwell 1990). This feature has also been observed here. Compared to other elements, Na and K

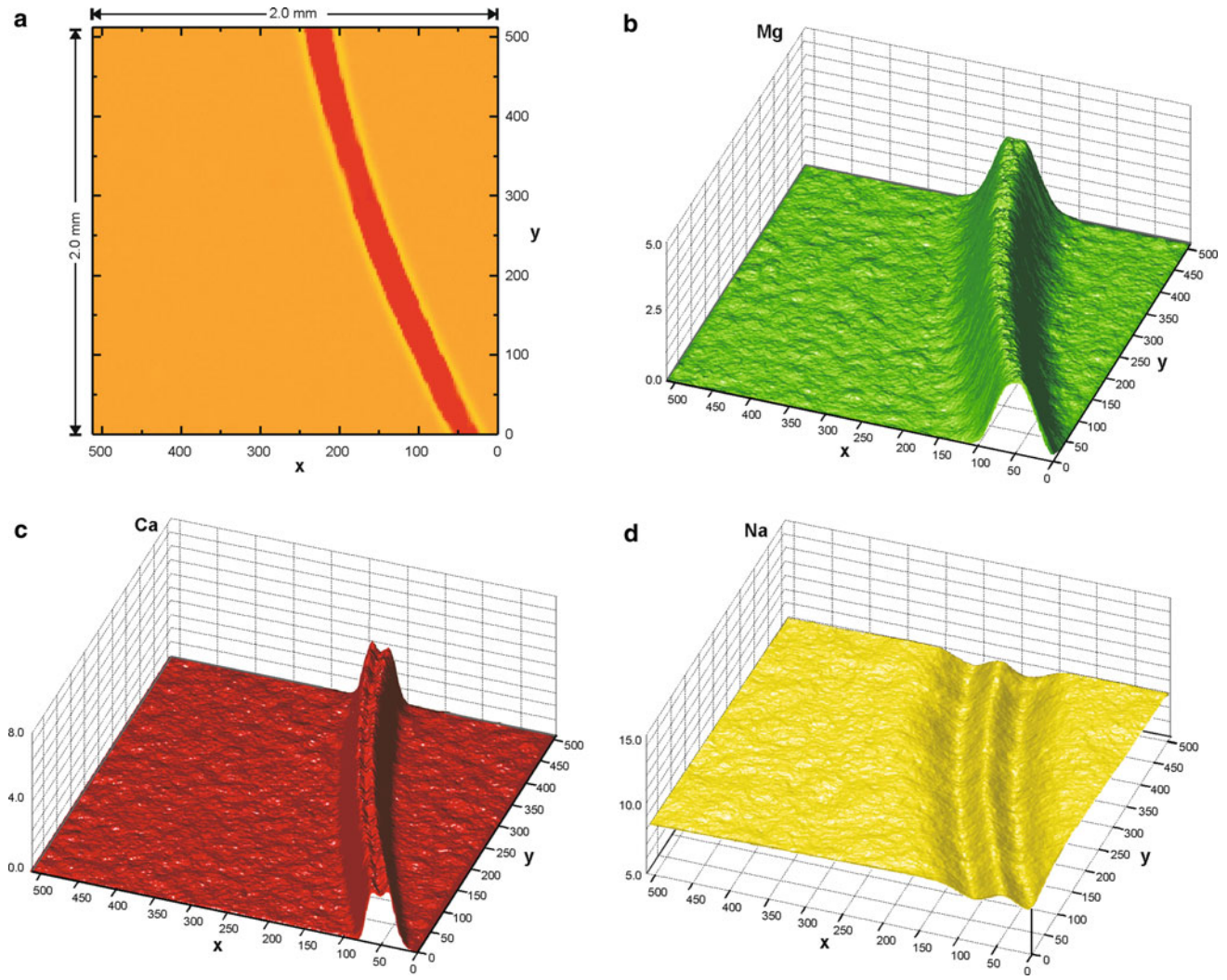

Fig. 11 **a** Color image of a curved portion of a filament (location of the analyzed area in the experimental sample is indicate by the black square in Fig. 5b; **b–d** compositional variability of Mg, Ca and Na, reported as 3D-graphs, in which the x and y coordinate represent the spatial dimensions of the mapped area **a** and the z coordinate reports the concentration of each considered element

show a higher density of measured values close to the hybrid composition (Fig. 8). This implies that not all elements attain the hybrid concentration at the same time (Fig. 10), generating a diffusive fractionation of chemical elements and producing complex non-linear patterns in binary plots (Fig. 9). This feature depends on the ability of each element to spread across the mixing system, as already observed in numerical simulations and natural samples (e.g. Perugini et al. 2008; De Campos et al. 2008). In addition, the process of "differential" diffusion for different chemical elements is superimposed to a complex pattern of lamellar structures, generated by the chaotic mixing process, which changes continuously with time, due to the stretching and folding of different melts. The combination of mechanical (stretching and folding) and chemical (multi-component diffusion) processes enhances the complexity of the process. Compositional fields in the magmatic system are being continuously re-modulated, strongly amplifying the effect of the different mobility of elements, in producing highly heterogeneous volumes of melts, even at short mixing times.

The further point worth highlighting is the disappearance of the original end-member compositions in those regions characterized by intimate mixing. Here, the production of large amounts of interfacial areas between melts via stretching and folding processes strongly enhances chemical diffusion leading to a dramatic shift of end-member compositions toward intermediate values. Noteworthy is the fact that this process occurred in the experimental system in less than 2 h, illustrating the extremely high efficiency of chaotic dynamics in modulating the compositional fields in the experimental system.

Petrological implications

The first petrological implication arising from the presented experimental work regards the ability of melts to mix even at high-viscosity ratios (of the order of 10^3). To date, according to previous studies (e.g. Jellinek et al. 1999; Sparks and Marshall 1986; Bateman 1995), it was thought that the "magmatological configuration" replicated in our experiment would have been characterized by null mixing efficiency, i.e. the viscosity ratio between the two melts is too high to allow the melts to efficiently mix. Results from our experiment clearly indicates that the mixing process can occur even under high-viscosity contrast, thus extending significantly the spectrum of geological conditions under which magma mixing processes can operate.

The magma mixing experiment presented in this contribution also offers new insights into the complex processes operating during mixing of magmas. It is shown that under fully chaotic dynamic conditions, the different chemical elements may become highly non-correlated even at short mixing timescales. This feature is tightly linked to the coupled action of stretching and folding dynamics between interacting magmas and the onset of complex chemical diffusion processes, including uphill diffusion. The formation of wide surface areas between different silicate melt filaments (i.e. magmas) reduces the length scale, diffusion becomes progressively more efficient.

Here, magma mixing is shown to be complex on short-length scale (i.e. experiments are conducted on cm-scale). But can the results be extended to natural magmatic systems? Although the possible applicability to natural magma mixing systems may be not straightforward, recent studies indicate that the magma mixing process is likely to generate fractal compositional patterns, independently of length scales (Perugini et al. 2003; Petrelli et al. 2006). The "scale-invariance" of filament thickness distribution of Fig. 6 also supports the conclusions of these studies: structures generated by magma mixing occur as a non-linear cascade of events generating compositional gradients over a large range of scales, down to the micrometer length scale. At such a length scale, chemical diffusion becomes very efficient, triggering a feedback process that, starting from the micro-scale, can amplify non-linearly the development of compositional heterogeneities up to the macro-scale. It follows that, at least from a conceptual point of view, the compositional variability observed in the magma mixing experiment presented here may also be applied to larger systems.

Thus, the mixing of magmas is a process that can virtually occur at any stage in the life span of a magmatic system and it does not necessarily require the presence of end-members generated from different sources (e.g. mantle and crustal derived melts; Fig. 12a). In fact, chaotic mixing processes will take place whenever chemical and also temperature gradients are present in the magmatic system. This implies that petrological processes such as fractional crystallization, assimilation and partial melting, which inevitably cause both chemical and temperature gradients, may be affected by chaotic mixing processes. Fractional crystallization tends to occur along the cooler walls (Fig. 12b) and depletes the magma in those elements incorporated into the crystals. Assimilation of country rocks (Fig. 12c) causes a chemical gradient from the core to the edge region. Anatexis or partial melting of a solid rock source similarly generates compositional and temperature gradients (Fig. 12d) as well as melt migration in fracture/channel networks (Fig. 12e). It is also possible that all these processes may act together strongly amplifying the interplay between mixing dynamics and chemical diffusion, inducing a considerable inhomogeneity in magmatic systems.

Therefore, chaotic mixing can generate pockets of magmas with highly heterogeneous geochemical compositions changing in space and time. The enrichment or depletion of chemical elements is a function of both: (1) their ability to spread within the mixing system and, (2) mixing dynamics. This may pose serious problems to the interpretation of petrogenetic processes and may undermine many classical geochemical models (e.g. magma mixing, assimilation plus fractional crystallization, etc.), widely used in petrological research. This is because most of these models do not consider time and space. The magmatic system is assumed to be completely homogeneous at any instant and everywhere during its evolution. Our results clearly indicate that in the presence of compositional gradients (i.e. volumes of magmas with different compositions), this is not the case and that highly heterogeneous volumes of melts, whose composition can be strongly influenced by the mixing process, can coexist in the same system in space and time.

The fact that chaotic mixing of magmas can trigger a diffusive fractionation processes at short-length scale opens an additional key question regarding the potential implication of such a process on small-scale petrological studies. In this respect, diffusive fractionation may have consequences regarding the reliability of analysis of small volumes of "magmatic systems", such as, for instance, melt inclusions hosted in minerals. Melt inclusions are unquestionably a new paradigm in modern igneous petrology, and their applicability to igneous systems had a strong impact on present understanding of magmatic processes. However, our results indicate that, at the micrometric length scale, small volumes of magmas are strongly influenced by the coupled action of chemical diffusion and chaotic flow fields and, hence, they may not represent magmas de facto

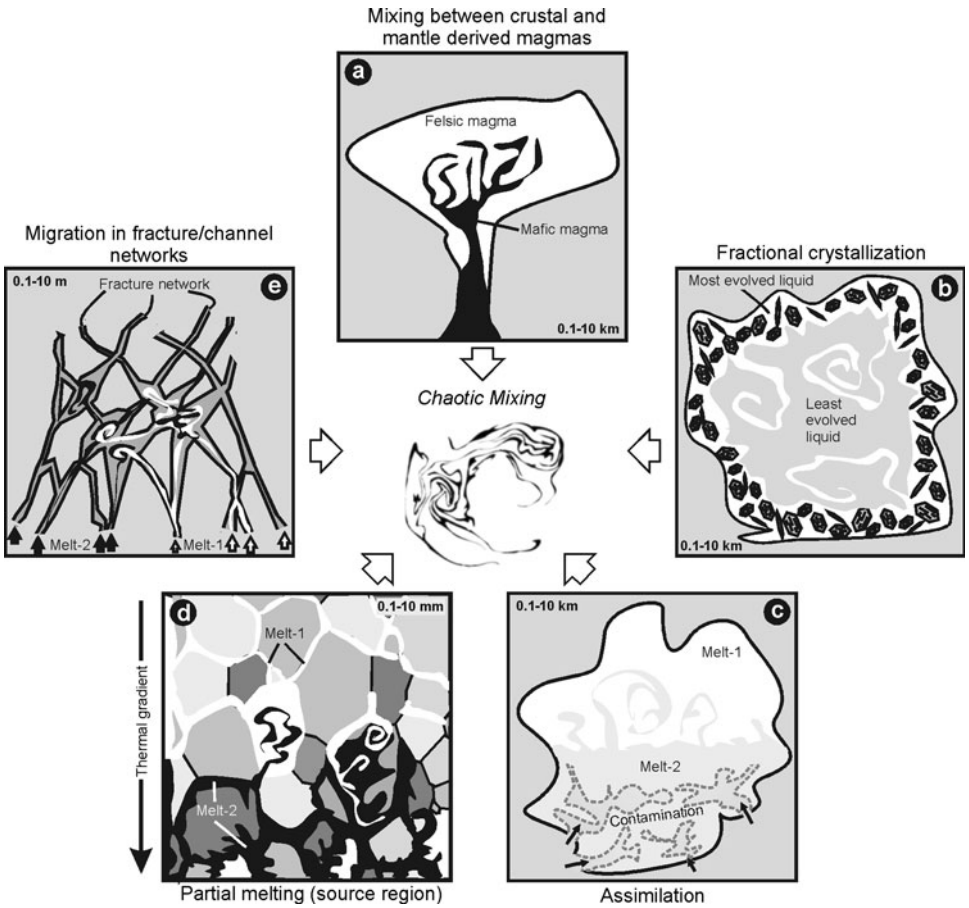

Fig. 12 Schematic drawing of some processes that can potentially generate compositional gradients in igneous systems and, thus, induce the development of chaotic mixing processes among the different melts

present in the magmatic system. On the contrary, their compositions may have experienced a diffusive fractionation process. If such melts were trapped as inclusions, they would provide misleading information about original melt compositions. The same arguments may be also applied to any case in which chemical element abundances are measured on volcanic glasses by micro-analytical techniques.

Conclusions

In this work, we presented a chaotic mixing experiment performed using high viscosity and temperature melts, with rheologic and physical properties similar to those of contrasting magmas. The experiment has been performed by developing a new device, in which we have full control of the flow fields developing in the mixing system.

Optical analysis of post-experimental samples reveals a complex pattern of mingled filaments forming a scale-invariant (i.e. fractal) distribution down to the μm-scale, as commonly observed in natural samples. This is due to the development in space and time of stretching and folding of the two melts. Chemical analysis shows strong non-linear correlations in inter-elemental plots. The original end-member compositions have nearly entirely disappeared from the filaments.

From a kinematic point of view, the experimental system possesses all building blocks of real magma mixing systems, including the development of chaotic dynamics and the generation of mixing patterns down to the micrometric length scale. These features make our experimental device a new reliable template for the study of magma mixing processes, whose results may be directly extrapolated to natural systems.

The results emerging from this first experiment highlight the importance of chaotic mixing processes in modulating the compositional fields of a mixing bimodal magmatic system. This modulation is tightly connected to the different ability of chemical elements to spread across the mixing system by chemical diffusion which, in turn, is governed by the generation of compositional gradients at different length scales. This phenomenon is associated with the development of wide interfacial areas (i.e. filament-like regions) in those regions of intricate mingling. The development of this process in space and time triggers a

diffusive fractionation of the different elements. Generated melt filaments are highly heterogeneous. In these filaments, the original compositions of end-members taking part in the mixing process are rapidly lost.

The observed compositional variability has been obtained by performing a short time-scale experiment at very low *Re* using melts with a high-viscosity ratio. This indicates that chaotic mixing of magmas can be a very efficient process in modulating the compositional fields in igneous systems, even under extreme rheologic conditions and absolutely laminar fluid-dynamic regime. It is worth noting that the experiment presented in this work is an 'extreme experiment', since most of melt fraction is constituted by a high-viscosity melt and only a small amount of lower viscosity mafic melt is present. One of the reasons for using this experimental configuration was motivated by the fact that we wanted to test the ability of our device in working under such conditions. The successful execution of the experiment may open new frontiers in the study of the complex behavior inherent to magma mixing processes, in which the interplay between advection (i.e. stretching and folding dynamics) and diffusion of multi-component materials is to be expected and understood. Now this complexity can be addressed in the laboratory.

Although in this contribution we utilized our experimental device to study the onset of mixing processes between completely different melts (i.e. felsic-mafic), it can also be used to gain information in general about those igneous processes, in which chemical gradients are generated and mixing processes are likely to occur (anatexis, fractional crystallization, xenolith assimilation, etc.). Using different volumes of melts, prepared according to the compositions that would be expected to occur under different petrogenetic conditions and, mixing them with our device, might provide the opportunity to study if and how the development of chaotic mixing processes would influence the compositional fields in such systems.

The experiment presented in this work is hopefully the first of a series in which different configurations will be tested in order to understand how the variation of a number of parameters can influence the development of mixing processes. In particular, future work will be focused on using different proportions of the felsic and mafic melts at different mixing times and experimental protocols.

Acknowledgments We thank P. Courtial for advice in sample preparation and T. K. Fehr for assistance with the microprobe. We also thank Jon Blundy, Jan Lavallée and two unknown reviewers for valuable comments and suggestions to a first version of this manuscript. This project was supported by INGV Campi Flegrei Unrest project (Italy), DFG- Project DI 431/31-1, AOBJ: 564369 and MIUR (Ministero dell'Istruzione, dell'Università e della Ricerca). DB Dingwell acknowledges a Research Professorship (LMU Excellent) of the Bundesexellenzinitiative.

References

Akonur A, Lueptow RM (2002) Chaotic mixing and transport in wavy Taylor-Couette flow. Phys D 167:183–196

Allègre CJ, Turcotte DL (1986) Implications of a two-component marble cake mantle. Nature 323:123–127

Aref H, El Naschie MS (1995) Chaos applied to fluid mixing. Pergamon Press, Reprinted from Chaos, Solutions and Fractals 4 Exeter

Baker D (1990) Chemical interdiffusion of dacite and rhyolite: anhydrous measurements at 1 atm and 10 kbar, application of transition state theory, and diffusion in zoned magma chambers. Contrib Mineral Petrol 104:407–423

Bateman R (1995) The interplay between crystallization, replenishment and hybridization in large felsic magma chambers. Earth Sci Rev 39:91–106

Bergantz GW (2000) On the dynamics of magma mixing by reintrusion: implications for pluton assembly processes. J Struct Geol 22:1297–1309

Bindeman IN, Davis AM (1999) Convection and redistribution of alkalis and trace elements during the mingling of basaltic and rhyolitic melts. Petrology 7:91–101

Blundy JD, Sparks RSJ (1992) Petrogenesis of mafic inclusions in granitoids of the Adamello massif, Italy. J Petrol 33:1039–1104

Bunsen R (1851) Über die Prozesse der vulkanischen Gesteinsbildungen Islands. Ann Phys 83:197–272

Chakraborty S (1995) Diffusion in silicate melts. In: Stebbins JF, McMillan PF, Dingwell DB (eds) Structure, dynamics and properties of silicate melts. Rev Mineral 32:411–503

Chakraborty S, Dingwell DB, Rubie DC (1995) Multicomponent diffusion in ternary silicate melts in the system K_2O–$Al_2O_3SiO_2$: II. Mechanisms, systematics, and geological applications. Geochim Cosmochim Acta 59:265–277

Christofides G, Perugini D, Koroneos A, Soldatos T, Poli G, Eleftheriadis G, Del Moro A, Neiva AM (2007) Interplay between geochemistry and magma dynamics during magma interaction: an example from the Sithonia Plutonic complex (NE Greece). Lithos 95:243–266

De Campos CP, Mendes J, Ludka I, de Medeiros S, de Moura JC, Wallfass C (2004a) A review of the Brasiliano magmatism in southern Espírito Santo, Brazil, with emphasis on post-collisional magmatism. In: Weinberg R, Trouw R, Fuck R, Hackspacher P (eds) The 750-550 Ma Brasiliano event of South America. J Virtual Explorer, Electronic Edition ISSN 1441–8142, 17: Paper 1

De Campos CP, Dingwell DB, Fehr KT (2004b) Decoupled convection cells from mixing experiments with alkaline melts from Phlegrean Fields. Chem Geol 213:227–251

De Campos CP, Perugini D, Dingwell DB, Civetta L, Fehr TK (2008) Heterogeneities in Magma Chambers: insights from the behavior of major and minor elements during mixing experiments with natural alkaline melts. Chem Geol 256:131–145

De Campos CP, Ertel-Ingrisch W, Perugini D, Dingwell DB, Poli G (2010) Chaotic mixing in the system earth: mixing granitic and basaltic liquids. In: Skiadas CH, Dimotikalis I (eds) Chaotic systems: theory and applications, selected papers from the 2nd chaotic modeling and simulation international conference (CHAOS2009). Int Publ Com, pp 51–58

De Rosa R, Donato P, Ventura G (2002) Fractal analysis of mingled/mixed magmas: an example from the Upper Pollara eruption (Salina Island, southern Tyrrhenian Sea, Italy). Lithos 65:299–311

Dingwell DB (1990) Effects of structural relaxation on cationic tracer diffusivities in silicate melts. Chem Geol 82:209–216

Dingwell DB, Virgo D (1987) The effect of oxidation state on the viscosity of melts in the system Na_2O-FeO-Fe_2O_3-SiO_2. Geochim Cosmochim Acta 51:195–205

Dingwell DB, Virgo D (1988) Viscosities of melts in the Na_2O-FeO-Fe_2O_3-SiO_2 system and factors controlling relative viscosities of fully polymerized silicate melts. Geochim Cosmochim Acta 52:395–403

Dingwell DB, O'Neill HStC, Ertel W, Spettel B (1994) The solubility and Oxidation state of Ni in silicate melt at low oxygen fugacities: results using a mechanically assisted equilibration technique. Geochim Cosmochim Acta 58:1967–1974

Dingwell DB, Hess KU, Romano C (1998) Extremely fluid behavior of hydrous peralkaline rhyolites. Earth Planet Sci Lett 158:31–38

Eichelberger JC (1978) Andesitic volcanism and crustal evolution. Nature 275:21–27

Eichelberger JC (1980) Vesiculation of mafic magma during replenishment of silicic magma reservoirs. Nature 288:446–450

Flinders J, Clemens JD (1996) Non-linear dynamics, chaos, complexity and enclaves in granitoid magmas. Trans R Soc Edinburgh Earth Sci 87:225–232

Fourcade S, Allègre C (1981) Trace elements behavior in granite genesis: a case study: the calc-alkaline plutonic association from the Querigut Complex (Pyrénées, France). Contr Mineral Petrol 76:177–195

Galaktionov OS, Anderson PD, Peters GWM (2002) Structure development during chaotic mixing in the journal bearing flow. Phys Fluids 14:3009–3017

Giordano D, Russell JK, Dingwell DB (2008) Viscosity of magmatic liquids: a model. Earth Planet Sci Lett 271:123–134

Hofmann AW (1980) Diffusion in natural silicate melts: a critical review. In: Hargraves RB (ed) Physics of magmatic processes. Princeton University Press, Princeton 9:385–417

Huppert HE, Sparks RS (1984) Double-diffusive convection due to crystallization in magmas. Am Rev Earth Planet Sci 12:11–37

Janoušek V, Bowes DR, Rogers G, Farrow CM, Jellinek E (2000) Modelling diverse processes in the petrogenesis of a composite batholith: the Central Bohemian Pluton, Central European Hercynides. J Petrol 41:511–543

Jellinek AM, Kerr RC, Griffiths RW (1999) Mixing and compositional stratification produced by natural convection. 1. Experiments and their application to earth's core and mantle. J Geoph Res 104:7183–7201

Kouchi A, Sunagawa I (1984) A model for mixing basaltic and dacitic magmas as deduced from experimental data. Contrib Mineral Petrol 89:17–23

Kratzmann DJ, Carey S, Scasso R, Naranjo JA (2009) Compositional variations and magma mixing in the 1991 eruptions of Hudson volcano. Chile Bull Volcanol 71:419–439

Lange RA, Carmichael ISE (1987) Densities of Na2O-K2O-CaO-MgO-FeO-Fe2O3-Al2O3-TiO2-SiO2 liquids: new measurements and derived partial molar properties. Geochim Cosmochim Acta 51:2931–2946

Langmuir CH, Vocke RDJ, Hanson GM, Hart SR (1978) A general mixing equation with application to the Icelandic Basalts. Earth Planet Sci Lett 37:380–392

Lautze NC, Houghton BF (2007) Linking variable explosion style and magma textures during 2002 at Stromboli volcano, Italy. Bull Volcanol 69:445–460

Leonard G, Cole J, Nairn I, Self S (2002) Basalt triggering of the c. AD 1305 Kaharoa rhyolite eruption, Tarawera Volcanic Complex, New Zealand. J Volcanol Geotherm Res 115:461–486

Liu M, Peskin RL, Muzzio FJ, Leong CW (1994) Structure of the stretching field in chaotic cavity flows. Am Inst Chem Eng J 40:1273–1286

Mungall J, Dingwell DB (1997) Actinide tracer diffusion in a haplogranitic melt. Geochim Cosmochim Acta 61:2237–2246

Murphy MD, Sparks RSJ, Barclay J, Carroll MR, Lejeune AM, Brewer TS, Macdonald R, Black S, Young S (1998) The Role of Magma Mixing in Triggering the Current Eruption at the Soufriere Hills Volcano, Montserrat, West Indies. Geophys Res Lett 25:3433–3436

Muzzio FJ, Meneveau C, Swanson PD, Ottino JM (1992) Scaling and multifractal properties of mixing in chaotic flows. Phys Fluids A4:1439–1456

Oldenburg CM, Spera FJ, Yuen DA, Sewell G (1989) Dynamic mixing in magma bodies: theory, simulations and implications. J Geophys Res 94:9215–9236

Ott E, Antonsen TM Jr (1989) Chaotic fluid convection and the fractal nature of passive scalar gradients. Phys Rev Lett 61:2839–2842

Ottino JM (1989a) The kinematics of mixing: stretching, chaos and transport. Cambridge University Press, Cambridge

Ottino JM (1989b) The mixing of fluids. Sci Am 260:56–67

Ottino JM, Leong CW, Rising H, Swanson PD (1988) Morphological structures produced by mixing in chaotic flows. Nature 333:419–425

Perugini D, Poli G, Mazzuoli R (2003) Chaotic advection, fractals and diffusion during mixing of magmas: evidence from lava flows. J Volcanol Geotherm Res 124:255–279

Perugini D, Ventura G, Petrelli M, Poli G (2004) Kinematic significance of morphological structures generated by mixing of magmas: a case study from Salina Island (Southern Italy). Earth Planet Sci Lett 222:1051–1066

Perugini D, Petrelli M, Poli G (2006) Diffusive fractionation of trace elements by chaotic mixing of magmas. Earth Planet Sci Lett 243:669–680

Perugini D, De Campos CP, Dingwell DB, Petrelli M, Poli G (2008) Trace element mobility during magma mixing: preliminary experimental results. Chem Geol 256:146–157

Petrelli M, Perugini D, Poli G (2006) Time-scales of hybridisation of magmatic enclaves in regular and chaotic flow fields: petrologic and volcanologic implications. Bull Volcanol 68:285–293

Poli G, Perugini D (2002) Strange attractors in magmas: evidence from lava flows. Lithos 65:287–297

Pouchou L, Pichoir F (1984) A new model for quantitative X-ray microanalysis: Part I: Applications to the analysis of homogeneous samples. Rech Aerosp 3:13–38

Roeder PL (1974) Activity of Iron and Olivine solubility in Basaltic liquids. Earth Planet Sci Lett 23:397–410

Snyder D, Tait SR (1998) The imprint of basalt on the geochemistry of silicic magmas. Earth Planet Sci Lett 160:433–445

Solgadi F, Moyen JF, Vanderhaeghe O, Sawyer EW, Reisberg L (2007) The role of crustal anatexis and mantle-derived magmas in the genesis of synorogenic Hercynian granites of the Livradois area, French Massif Central. Can Min 45:581–606

Sparks SRJ, Marshall LA (1986) Thermal and mechanical constraints on mixing between mafic and silicic magmas. J Volcanol Geotherm Res 29:99–124

Sparks SRJ, Sigurdsson H, Wilson L (1977) Magma mixing: a mechanism for triggering acid explosive eruptions. Nature 267:315–318

Swanson PD, Ottino JM (1990) A comparative computational and experimental study of chaotic mixing of viscous fluids. J Fluid Mech 213:227–249

Toramaru A, Takazawa E, MOrishita T, Matsukage K (2001) Model of layering formation in the mantle peridotite (Horoman, Hokkaido, Japan). Earth Planet Sci Lett 185:299–313

Watson BE, Jurewicz SR (1984) Behavior of alkalies during diffusive interaction of granitic xenoliths with basaltic magma. J Geol 92:121–131

Welander P (1955) Studies on the general development of motion in a two dimensional, ideal fluid. Tellus 7:141–156

Wiebe RA (1994) Silicic magma chambers as traps for basaltic magmas: the Cadillac mountain intrusive complex, Mount Desert island, Maine. J Geol 102:423–427

Wilson M (1989) Igneous petrogenesis. Kluwer, Dordrecht